

Transport Limitations in Electrodeposition for LIGA Microdevice Fabrication

S. K. Griffiths, R. H. Nilson, R. W. Bradshaw, A. Ting
W. D. Bonivert, J. T. Hachman and J. M. Hruby

Sandia National Laboratories
Livermore, California 94551-0969

ABSTRACT

To better understand and to help optimize the electroforming portion of the LIGA process, we have developed one and two-dimensional numerical models describing electrodeposition of metal into high aspect-ratio molds. The one-dimensional model addresses dissociation, diffusion, electromigration, and deposition of multiple ion species. The two-dimensional model is limited to a single species, but includes transport induced by forced flow of electrolyte outside the mold and by buoyancy associated with metal ion depletion within the mold. To guide model development and to validate these models, we have also conducted a series of laboratory experiments using a sulfamate bath to deposit nickel in cylindrical molds having aspect ratios up to twenty-five. The experimental results indicate that current densities well in excess of diffusion-limited currents may still yield acceptable morphologies in the deposited metal. However, the numerical models demonstrate that such large ion fluxes cannot be sustained by convection within the mold resulting from flow across the mold top. Instead, calculations suggest that the observed hundred-fold enhancement of transport probably results from natural convection within the molds and that buoyancy-driven flows may be critical to metal ion transport even in micron-scale features having very large aspect ratios. Taking advantage of this enhanced ion transport may allow order-of-magnitude reductions in electroforming times for LIGA microdevice fabrication.

Keywords: LIGA, electrodeposition, electroforming, transport

1. INTRODUCTION

LIGA, an acronym from the German words for lithography, electroforming and molding, is a promising new process for producing high aspect-ratio metal microdevices having micron to millimeter features.^{1,2,3} In LIGA, high-energy x-ray lithography is used to produce a deep non-conducting mold^{4,5,6} that is subsequently filled by means of electrodeposition to produce metal parts. The final step in true LIGA is injection molding for mass production, here using the electroformed metal part as a mold. Currently under worldwide development, this process offers a means to manufacture high resolution, high aspect-ratio devices including microscale valves, motors, solenoid actuators, and gear trains. Such devices cannot be fabricated either by silicon micromachining or by precision machine tool operations.

Most previous research in LIGA has focused on lithography and developing.^{4,5,6} Electrodeposition for LIGA has been relatively neglected, despite several serious problems. Large-scale voids in the deposited metal occur frequently and often without apparent cause. Similarly, local deposition rates within a mold vary widely depending on local feature sizes and on the macro-scale geometry of collections of features. Such local variations in deposition rate lead to uneven mold filling and, eventually, to regions of the mold that cannot be filled completely. Further, deposition surfaces are often rough or wavy, necessitating post-deposition polishing to produce parts having acceptable tolerances and surface finish.

Further author information –

S.K.G. (correspondence): Email: skgriff@sandia.gov

Sandia National Laboratories LIGA Web site: <http://daytona.ca.sandia.gov/LIGA/>

Many of these problems likely result from transport limitations that arise because the electrolyte in deep mold features may remain nearly stagnant, despite vigorous bath stirring. In such a transport-limited growth process, the deposition surface will typically roughen and become unstable as deposition rates are increased and ion depletion becomes significant.^{7,8} Hydrogen gases may also be generated when ion depletion is significant, leading to a second mechanism for anomalies in the deposition surface. Although it may be possible to avoid these nonuniformities by reducing deposition rates, the electroforming portion of the LIGA process presently may require days or even weeks. Thus further reducing deposition rates may become burdensome to overall LIGA processing cost and cycle time. In addition, the very low overpotentials associated with low current densities and low deposition rates may themselves produce unacceptable metal morphologies.

To help understand these problems and to help optimize the process, we have developed a pair of numerical models. The first is a one-dimensional model describing the electric field and diffusion, dissociation, electromigration, and the deposition kinetics of multiple ion species. This model is used to compute spatial variations in ion concentrations, local pH and associated surface deposition rates based on bath chemistry, mold height and applied current for cases in which electrolyte within the feature may be considered stagnant. Both steady and transient solutions can be computed using this multi-species model. The second is quasi-steady two-dimensional model addressing forced and buoyancy-driven convection, as well as diffusion, outside and within the mold. This second model considers only a single species, but includes deposition kinetics of a form similar to those of the multi-species model. Together, these two models address all key physics of the electrodeposition of metal into high aspect-ratio molds.

In parallel with model development, we have also conducted a series of laboratory experiments. These experiments were designed to provide well characterized boundary conditions in order to obtain both qualitative and quantitative insight into the transport processes inside mold features. By observing the deposit morphology for various mold depths, aspect ratios and plating currents, these experimental results have identified the acceptable operating conditions for nickel deposition from a sulfamate bath. Comparison of these observations with our numerical results has helped to guide model development and to validate the numerical results. This combined experimental and numerical approach has revealed that buoyancy-driven ion transport can enhance deposition rates by an order-of-magnitude or more relative to those possible by diffusion alone.

2. GOVERNING EQUATIONS: MULTI-SPECIES TRANSPORT

To model electrodeposition in LIGA molds, we consider the simplified geometry of a single mold feature as shown in Fig. 1. Far from the mold top, $y \gg h$, species concentrations are at uniform values and the fluid moves with a uniform speed from left to right. This uniform far-field flow produces a linear gradient of the fluid speed in a boundary layer just above the mold top and upstream of the feature. The shear along the mold top is transmitted to the fluid at the top of the feature, and this may drive recirculating convection cells below. However, as later discussed the effects of this forced convection are negligible when the aspect ratio is large, even when fluid speeds at the mold top are also very large.

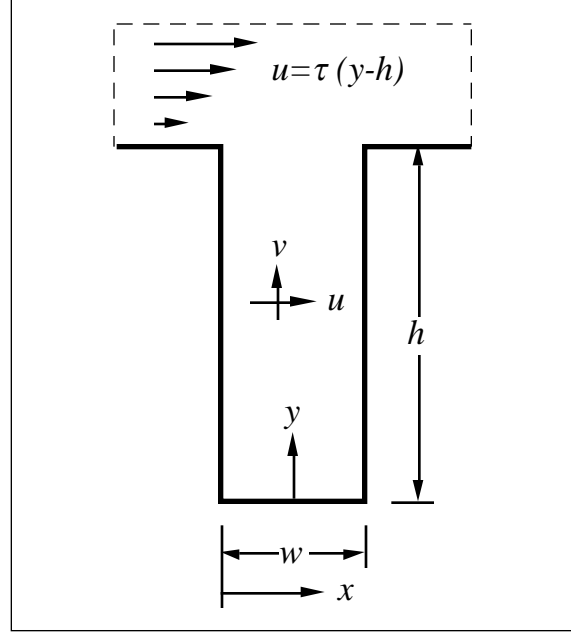
We first address the case in which buoyancy forces and the associated natural convection within the feature can be neglected. The conditions under which this is appropriate are also discussed later. In the absence of natural convection, electrodeposition inside the feature is nearly one dimensional, provided that the aspect ratio of the feature $A = h/w$ is large. For this reason, the electric field and species transport equations may be written as second-order differential equations in time and the spatial position along the mold. Species concentrations, c_i , within the feature are governed by species conservation equations,^{9,10,11}

$$\frac{\partial c_i}{\partial t} + \nabla \cdot \mathbf{J} = S_i \quad (1)$$

where t is time, \mathbf{J} are the species fluxes, and S_i are volumetric sources or sinks associated with homogeneous reactions. Note that the concentrations c_i represent both neutral and ionic species, and that ionic species may be both metallic and nonmetallic. The species fluxes are given by⁹

$$\mathbf{J} = -D_i \nabla c_i + e v_i z_i c_i \mathbf{E} \quad (2)$$

Figure 1. Schematic of a LIGA mold feature. Such a feature may be either a trench or cylinder. Metal ions are carried from the mold top to the deposition surface at the feature bottom by convection, diffusion and ion drift due to the applied electric potential. The feature aspect ratio is given by $A = h/w$.



where D_i is the effective diffusivity of the i th species, e is the elementary charge, and z_i is the species charge number, and v_i is the ion mobility. The static electric field, \mathbf{E} , is governed by the Poisson equation relating the electric field to the local charge density. A common alternative to solving the Poisson equation is to enforce local electroneutrality. In this case, the electric field $\mathbf{E} = -\nabla V$ becomes an unknown constant to be determined as part of the overall solution, and the governing equation becomes

$$\sum_{i=1}^n z_i c_i = 0 \quad (3)$$

Like the Poisson equation, this condition of electroneutrality applies at every point in the concentration field, except within the Debye layer adjacent to each electrode. These regions are instead accounted for by the Butler-Volmer kinetics relation.

Consistent with the assumption of an electrostatic field, there may be no time-dependent variation in the local charge density. This is equivalent to

$$\nabla \cdot \mathbf{I} = \nabla \cdot \left(\sum_{i=1}^n \mathbf{I}_i \right) = \nabla \cdot \left(\sum_{i=1}^n z_i \mathbf{J} \right) = 0 \quad (4)$$

Currents associated with each ion species can be computed easily after the basic transport equations have been solved. These are given as the sum of the two contributions to the ion fluxes,

$$\mathbf{I}_i = F z_i \mathbf{J} = -F z_i D_i \nabla c_i + F^2 v_i z_i^2 c_i \mathbf{E} \quad (5)$$

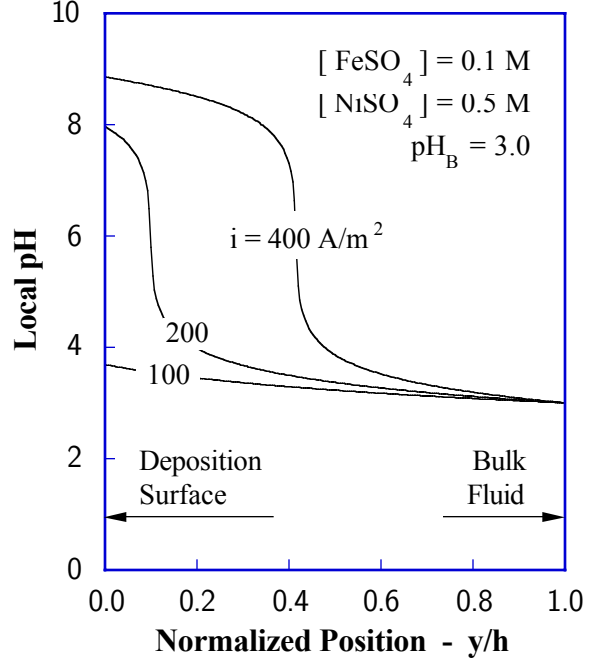
where \mathbf{I}_i is the current due to the i th species, and F is Faraday's constant.

Equation (4) closes the conservation equations for species and electric charge. For the case of diffusive transport considered just now, momentum equations are not required. Similarly, energy equations are everywhere replaced by an assumption that the temperature, T , is uniform and constant.

3. SAMPLE CALCULATIONS: DIFFUSIVE TRANSPORT

Figure 2 shows sample calculations of the local pH for codeposition of nickel and iron from a 0.5 M NiSO_4 and 0.1 M FeSO_4 bath at a pH of 3.¹² The height of the mold is 100 μm , and the total current is varied between 100 and

Figure 2. Local pH through mold thickness of a LIGA feature. The pH at the deposition surface (left) increases rapidly at current densities above 100 A/m². These currents are still well below the diffusion limited current of about 1100 A/m². High pH at deposition surface leads to poor metal morphology and hydrogen generation.



400 A/m². In Fig. 2 we see that the pH at the deposition surface (left of plot) remains nearly constant at the bath value up to a critical current density of about 100 A/m². The surface pH then abruptly climbs and the region of high pH moves off the surface toward the mold top as the current is further increased. The pH at the deposition surface is important in all plating processes since it affects the deposition morphology as well as the onset of hydrogen formation via hydrolysis.

An important consequence of these results is that the currents shown in Fig. 2 are well below the diffusion limited current for this mold height. This limiting current for a simple diffusion layer is given by

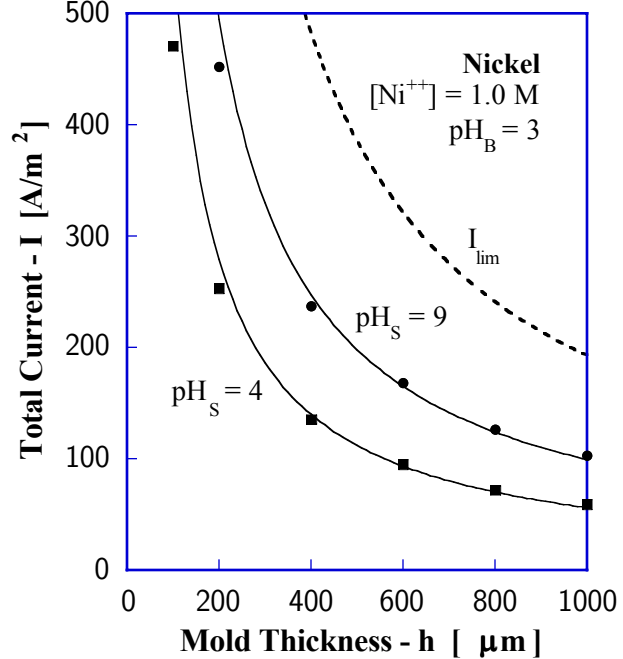
$$I_{\text{lim}} = 2F \frac{c_0 D}{h} \quad (6)$$

Based on a combined bath concentration of $c_0 = 0.6 \times 10^3 \text{ mol/m}^3$, $D \approx 10^{-9} \text{ m}^2/\text{s}$ and $h = 100 \text{ }\mu\text{m}$, the limiting current is $I_{\text{lim}} = 1100 \text{ A/m}^2$. Thus dramatic increases in the surface pH are evident when the imposed current is only about 20% of the limiting value.

Because pH at the deposition surface strongly affects the morphology of deposited metal, it provides one basis for selecting a desired current density. Since deposition rate is proportional to current (provided that current efficiencies remain near unity), the highest possible current is desired in order to minimize the total processing time. However, excessive current densities lead to poor morphology, so some optimum current must exist. To help identify these optimum currents for a sample problem, we have made a series of calculations for nickel deposition from a 1.0 M sulfate bath at an initial pH of three. In these calculations, the surface potential was adjusted to a point where the surface pH reached a specified value of either four or nine. The results of these calculations are shown in Fig. 3.

The symbols shown in Fig. 3 are the computed total currents corresponding to a given pH at the deposition surface, for a given mold thickness or height, h . The dashed curve in this figure is the diffusion limited current given by Eq. (6). The two solid curves are simply the diffusion limited current shifted downward by a fixed multiplicative factor. Currents along the solid curve for $\text{pH}_S = 4$ are 29% of the limiting values, while those for $\text{pH}_S = 9$ are 52% of the limiting values. The generally good agreement between these solid curves and the numerical results over a wide range of mold thicknesses indicates that the transport problem scales well with mold thickness, and that a given increase in surface pH will correspond roughly to given ratio of the actual and limiting currents. These results can therefore be scaled approximately to other bath compositions simply by increasing or decreasing the currents

Figure 3. Allowable total currents as a function of mold thickness, h . Numerical solutions (symbols) were obtained for currents yielding a specific pH at the deposition surface by iteratively adjusting the surface potential. The dashed curve is the diffusion limited current given by Eq. (6). Solid curves are fixed fractions of 0.29 ($\text{pH}_S = 4$) and 0.52 ($\text{pH}_S = 9$) of the diffusion limited current.



shown in proportion to the actual bath ion concentration. Moreover, plating solutions other than nickel sulfate will probably exhibit similar behavior since the effective binary diffusivities of all small ions in an aqueous solution is order 10^{-9} m^2/s . Only the addition of pH buffers to the plating bath is likely to have a strong influence on this conclusion.

4. EXPERIMENTAL RESULTS

Our experiments explore essential features of LIGA-like metal deposition under well characterized conditions that can be compared with theoretical calculations. A commercial nickel plating solution at a nominal temperature of 38 C was pumped through a Lucite channel having metal anodes and cathode molds mounted into opposing channel walls. A typical cathode mold consists of a PMMA disc having several identical drill-holes in which metal is deposited. A copper foil on the back of the mold serves as a common cathode for all of the holes. Following deposition, the foil is removed to permit extraction and weighing of deposits and visual examination of the deposition surface. The transparent mold also allows the observation of hydrogen bubble formation during plating. The hole diameter and mold thickness were varied to obtain aspects ratios ranging from 1.6 to 25.

Current densities varying from 11 to 1080 A/m^2 were applied to a number of molds to produce metal deposits in holes having diameters of 1.7, 3.2 and 6.4 mm and depths of 17 to 42 mm. The enlarged photos of Fig. 4 illustrate a severe degradation of surface morphology with increasing current density. Although smooth, uniform deposits were produced at 11 A/m^2 , several obvious defects were observed at 65 A/m^2 , and the deposition morphology became clearly unacceptable at currents above 400 A/m^2 . These current densities producing smooth uniform deposits are considerably smaller than the 200 to 300 A/m^2 commonly used to plate nickel on flat surfaces in well agitated baths, suggesting that the poor morphology is caused by accumulation of hydrogen and depletion of metal ions in the deep, stagnant holes of the molds.

Despite the differing appearances of the deposits shown in Fig. 4, the current efficiency was generally above 98%. The remaining current apparently produced gaseous hydrogen by reduction of hydrogen ions and water. While small (< 0.1 mm) bubbles were often seen detaching from the surface and rising upward through the bores, some bubbles remained attached throughout the plating experiments. In these cases, smooth curved surfaces were observed that replicated the shape of the attached bubble as the deposit grew around the obstruction. An example of such a cavity can be seen at the 11 o'clock position of the top row, right photograph in Fig. 4.

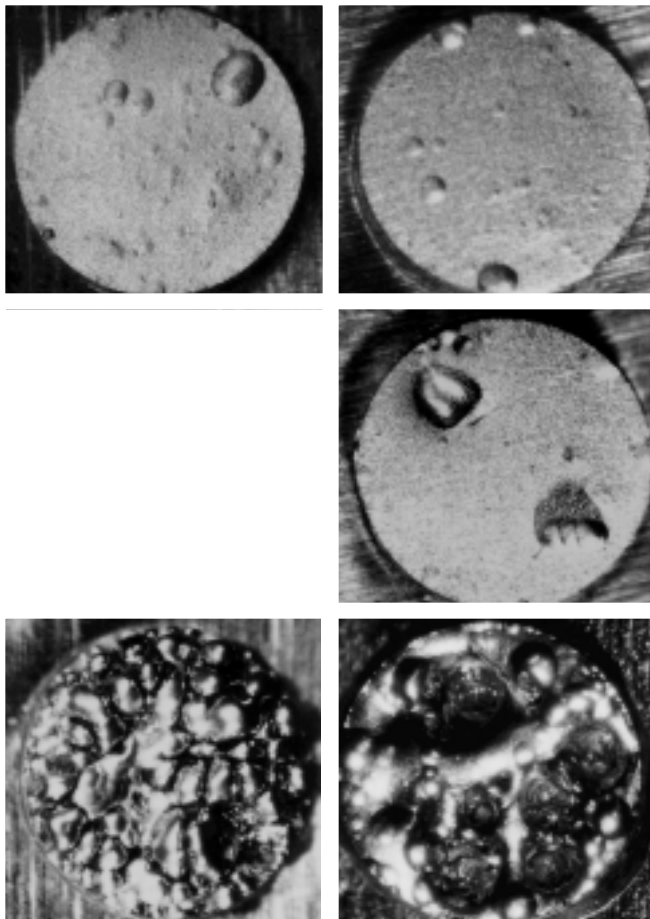


Figure 4. The effect of current density on the macroscopic morphology of nickel deposits on recessed cathodes for which $d = 1.7$ mm and aspect ratio was 25. Reading clockwise from top left, current densities are 108, 215, 323, 430, and 646 A/m². The images were obtained by optical microscopy.

The most remarkable result of these experiments is that the measured maximum currents are ten to one hundred times greater than the diffusion-limited current given by Eq. (6). This may be seen in Table 1, which includes a Sherwood number representing the ratio of measured current to diffusion-limited current. We believe that these very large transport rates result from natural convection driven by metal ion depletion at the plating surface. To verify this hypothesis, we performed additional experiments in which the plating apparatus was turned upside down. In this inverted configuration, maximum plating currents were reduced by more than an order of magnitude, compared to those observed for an upward facing plating surface. Numerical calculations presented in the next section further verify that the enhanced transport probably results from fluid density reduction associated with metal ion depletion. Rising hydrogen bubbles could produce a similar effect, though probably not in the steady and repeatable manner observed in the experiments.

5. BUOYANCY-DRIVEN CONVECTION

Buoyancy-driven fluid motions and related transport processes have been extensively studied, particularly in heat transfer applications where the fluid density varies with the temperature. Although such temperature variations may exist in electroplating processes, the corresponding density variations are no greater than 0.3%, even for a temperature difference as large as 30 C. Of far greater importance is the local reduction in fluid density resulting from the depletion of metal ions at the plating surface. Removal of these heavy ions from the adjacent electrolyte reduces the local fluid density by as much as 10% when plating at relatively high rates from 1 M nickel baths. Because of its reduced density, the depleted electrolyte rises from an upward facing electrode, permitting the inflow of fresh electrolyte.

Cavity Diameter (mm)	Aspect Ratio	Current Density (asf)	Current Efficiency	Sherwood Number	Rayleigh Number
1.70	10	10	99.7	48.0	3.3×10^9
1.70	15	80	96.4	82.2	1.1×10^{10}
1.70	25	80	89.6	137.5	5.2×10^{10}
3.18	8	80	99.5	82.2	1.1×10^{10}
6.35	1.6	100	100.9	41.1	7.1×10^8

Table 1. Current efficiency and Sherwood number of nickel plating in cylindrical recesses having various aspect ratios. Values shown are for largest current density for each mold geometry.

Despite the relatively large density differences associated with ion depletion, there is very little mention of natural convection in the electroplating literature.^{13,14} This is because natural convection plays only a secondary role in conventional plating of flat surfaces; there fresh electrolyte is supplied to the plating surface by vigorous stirring of the bath. Such forced flows of electrolyte may also help to stir the upper portion of a LIGA feature such as a narrow trench or a hole. However, the strength of the this forced convective transport decreases logarithmically with the ratio of feature depth to width,^{15,16} making it nearly irrelevant for aspect ratios beyond three or four. Thus, only buoyancy-driven convection is important to electrodeposition in high aspect-ratio features.

Although the literature of heat and mass transfer includes hundreds of studies of natural convection, none deal directly with the configuration of interest here.¹⁷ Studies addressing slender LIGA-like domains are mainly concerned with transport induced by horizontal gradients of temperature and density. Conversely, previous studies exploring vertical density gradients have focused on relatively shallow layers, with experimental studies limited to a maximum aspect ratio of four and Rayleigh numbers orders of magnitude greater than those encountered in LIGA.¹⁸ Thus, the regime of interest for LIGA remains unexplored.

The equations describing steady-state conservation of mass for a nearly incompressible fluid containing multiple chemical species may be written

$$\nabla \cdot \mathbf{u} = 0 \quad (7)$$

$$\nabla \cdot (\mathbf{u}c) = \nabla \cdot (D\nabla c) \quad (8)$$

where $\mathbf{u} = u\mathbf{i} + v\mathbf{j}$ is the fluid velocity vector, c is the partial molar density of any chemical component, and D is the effective binary diffusivity for that species. Rather than solving continuity equations for all species of a complex bath, we now focus attention on a particular component that is largely responsible for density reduction at the plating surface. Thus, c will represent the concentration of a singular depositing metal ion.

Under the customary Boussinesq approximation, the fluid density is treated as though it were uniform except in evaluating the buoyancy force, $\rho\mathbf{g}$, appearing in the following statement of momentum conservation.

$$\rho(\nabla \times \mathbf{u}) \times \mathbf{u} = -\nabla p - \rho\mathbf{g} + \mu\nabla^2 \mathbf{u} \quad (9)$$

Here, p and μ are the pressure and the kinematic viscosity. For simplicity, the ion diffusivity and fluid viscosity are presumed uniform and the fluid density is assumed to vary linearly with the metal ion concentration. To isolate the effects of buoyancy, the electric field forces have been omitted from the momentum balance. As shown earlier, the associated ion drift velocities provide only a modest enhancement to diffusive transport under typical plating conditions.

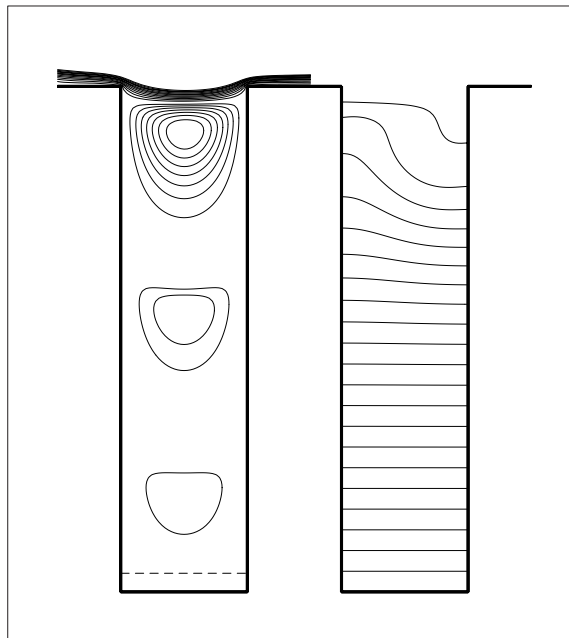


Figure 5. Stream lines and concentration isopleths for forced convection driven by horizontal flow above feature. Fluid speed within convective cells decreases by a factor of 10^3 from one cell to the next. Uniformly spaced horizontal isopleths indicate a condition of purely diffusive transport beneath the uppermost cell.

To facilitate numerical solution by finite difference methods, it is convenient to nondimensionalize all of the equations and to rewrite the momentum equation in terms of the normalized stream function and vorticity. The two parameters appearing in the resulting species and momentum conservation equations are the Rayleigh and Schmidt numbers; both are written below in terms of the dynamic viscosity $\nu = \mu/\rho_0$.

$$\text{Ra} = \frac{\Delta\rho g h^3}{\rho_0 D\nu} \quad \text{and} \quad \text{Sc} = \frac{\nu}{D} \quad (10)$$

Since the Schmidt number is typically of the order 10^3 for small ions in an aqueous solution, the advective vorticity transport is generally negligible. In this asymptotic regime, there is essentially no dependence of the solutions on the Schmidt number. The only remaining parameter is the Rayleigh number, a measure of the strength of the buoyancy-driven motion. For LIGA features having depths, h , ranging from 0.1 to 1.0 mm, the Rayleigh number is on the order of 10^5 to 10^8 . This estimate is based on a relative density difference of $\Delta\rho/\rho_0 = 0.1$, as appropriate for a 1 M nickel bath and full depletion of metal ions at the deposition surface. The actual value of the normalized surface concentration is, however, controlled by the boundary condition at the plating surface.

The preceding partial differential equations are solved numerically using a finite difference scheme on the T-shaped domain shown in Fig. 1. The lower rectangular part of the domain represents a trench-like LIGA feature of height h and width w . Since the side walls of the trench are electrical insulators, plating occurs only along the bottom surface.

6. SAMPLE CALCULATIONS: CONVECTIVE TRANSPORT

Figure 5 shows the calculated streamlines and concentration field for a flow driven by an external shear stress of $\tau^* = 10^4$, a Rayleigh number of zero, and an aspect ratio of $A = h/w = 4$. This normalized shear stress is roughly that produced at the top of a 1 mm deep LIGA feature by a fluid speed of 60 mm/s in a channel of height 20 mm, like that used in the laboratory experiments described earlier. Since the general problem of a shear-driven cavity has been studied previously,¹⁶ this example serves both to validate our numerical procedure and to illustrate shear driven flow in the absence of buoyancy. We see that the streamlines of the external flow bend slightly downward into the cavity, increasing the local shear stresses at the upper edges of the cavity. This is one of the reasons for applying the external boundary conditions well above the mold top, since the velocity, shear stress and species concentration at the top of the feature are not known beforehand.

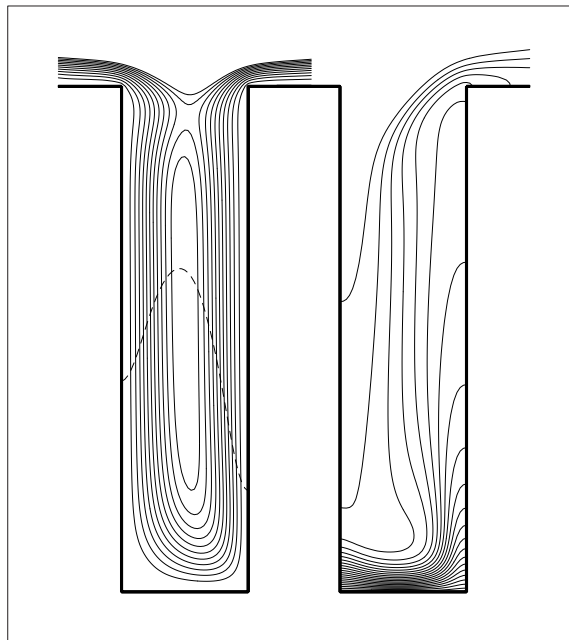


Figure 6. Stream lines and concentration isopleths for a buoyancy-driven flow with a Rayleigh number of 10^6 . Strong convective motion carries fresh electrolyte deep into feature, reducing the thickness of the diffusive boundary layer at the plating surface.

The shear-driven circulation within the trench of Fig. 5 consists of three counter-rotating cells, each having an aspect ratio of roughly 1.3. The stream line pattern within each cell is nearly identical, so long as the Reynolds number, $Re = uw/\nu$ is no greater than a few hundred. That criterion is well satisfied here since $Re = \tau^*/ScA^2 < 1$. Despite this similarity of flow pattern, the maximum fluid speeds within each circulation cell decreases by a factor of roughly 10^3 from one cell to the adjacent cell below. A contour plot of the ion concentration field is shown on the right side of Fig. 5. The equal spacing of concentration isopleths along most of the trench indicates that the concentration gradient is uniform, as required for steady state transport by diffusion alone. Wider spacing of the uppermost isopleths is indicative of strong convective transport in the upper circulation cell.

The Sherwood number, Sh is the ratio of the total vertical transport by convection and diffusion to that which would occur by diffusion alone. Continuity requires that the Sherwood number for a steady process must be the same at all elevations in the feature. It is most conveniently evaluated at the deposition surface where the vertical velocity must vanish and local transport occurs only by diffusion.

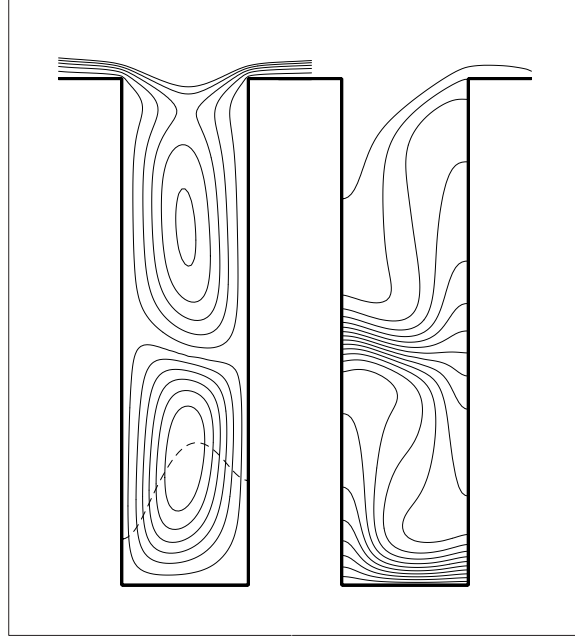
$$Sh = \left(\frac{h}{D\Delta C} \right) \frac{1}{w} \int_0^w D \frac{\partial C}{\partial y} dx = A \int_0^{1/A} \frac{\partial c^*}{\partial y^*} dx^* \quad \text{on} \quad y^* = 0 \quad (11)$$

Applying this definition to the calculation of Fig. 5 yields a Sherwood number of 1.2, indicating only a 20% improvement in transport over diffusion alone.

The fundamental limitation of forced convection transport in high aspect-ratio features is well illustrated by the example of Fig. 5. Even if the uppermost convective cell were perfectly mixed with a uniform concentration of $c^*=1$, the overall flux would still be limited by diffusion through the relatively stagnant lower region. The net effect of a strongly convective upper cell is a reduction in diffusion distance by a ratio of three to two, yielding a maximum Sherwood number of about 1.5. Further increases in the Sherwood number can only be obtained by convective transport in the second cell from the top. Since it rotates a thousand times slower than the cell above, a thousand-fold increase in the external shear force is needed to achieve significant convection in that cell and thereby increase the Sherwood number to a maximum of three. By this same reasoning, the external shear velocity would have to be increased by a factor of 10^{15} to obtain Sherwood numbers greater than two for an aspect ratio of ten.

Unlike external shear forces, buoyancy forces may induce strong vertical motions that are nearly independent of elevation. Such a flow field is illustrated in Fig. 6 for $Ra = 10^6$ and, as before, $\tau^* = 10^4$. In contrast to a shear

Figure 7. Bicellular convective motion for a Rayleigh number of 10^6 . Although this flow pattern is more stable than a single cell, the transport is inhibited by the presence of a diffusion layer at mid-height where ion species are exchanged between the two counter-rotating cells.



driven flow, only one elongated circulation cell is produced, rather than many cells of nearly unit aspect ratio. The relatively dense external flow now turns downward into the trench, then descends to the bottom where it loses some of its metal ions by diffusion to the plating surface. The depleted fluid then rises to the surface where it rejoins the external stream. The calculated circulation is counter clockwise, though a strong enough external shear would close the top of the cell and reverse its direction. Note that the streamlines of Fig. 6 are spaced uniformly in ψ^* , such that the volumetric flow rate between any adjacent streamlines is the same. Thus, the relatively uniform physical spacing of streamlines indicates that flow speeds are everywhere comparable, even in the turning region near the bottom.

The isopleths of Fig. 6 reveal a narrow boundary layer just above the deposition surface. In this region the fluid motion is essentially horizontal, requiring that the vertical flux be carried by diffusion alone. The local vertical gradient must thus be steeper here than in the upper region where the flux is carried advectively by opposing vertical streams having differing ion concentrations. These side-to-side differences in concentration are apparent in the nearly vertical, rather than horizontal, orientation of the isopleths at midheight. As the descending fluid approaches the plating surface, it compresses the isopleths on the left side, whereas the ascending fluid expands the isopleths on the right. This asymmetry of motion results in the asymmetric flux profile indicated by a dashed curve in the left frame of Fig. 6. The peak flux occurs near the center, where the horizontal velocity is greatest and the diffusion layer is thinnest. The vertical scale of this flux profile is the same as in the preceding Fig. 5, so the magnitude is clearly greater in the present buoyancy-driven flow.

The ion flux to the deposition surface for the case of Fig. 6 corresponds to a Sherwood number of about 14, exceeding that for the shear driven flow by more than a factor of ten. This level of enhancement is consistent with the concentration field, since the steep gradients are now confined to just 10% of the feature depth. Ion concentrations just above that layer are nearly equal to the bath concentration, shortening the diffusion distance by a factor of ten.

Cell structures in buoyancy-driven flows may be altered significantly by slight variations in boundary or initial conditions. For example, the bicellular pattern shown in Fig. 7 has the same Rayleigh number and the same external shear stress as the monocellular pattern of Fig. 7. In fact, the bicellular structure is the preferred steady state solution. The single cell shown earlier was obtained by tilting the axis of the feature slightly off of vertical. In that tilted orientation, the component of gravity acting across the feature pulls the heavier fluid toward the lower sidewall. Thus, the tilt disfavors a bicellular pattern in which the opposite rotation of the cells necessarily places the heavier fluid on opposite walls in the upper and lower cells.

Multicellular flows are generally less efficient than single cell structures in transporting ion species. In the preceding examples, the Sherwood number decreased by almost a factor of three, from 14 to 5, between the single and multiple cells driven by nearly identical shear and buoyancy forces. The primary reason for this is apparent in the ion concentration fields of Figs. 6 and 7. Although both configurations have boundary layers at the deposition surface, only the bicellular flow has an additional diffusion layer at midheight. Here, steep concentration gradients are needed for diffusion exchange of ionic species between the upper and lower cells. Advection cannot enhance this exchange since no flow crosses between the two cells. The presence of two diffusion layers, rather than one, reduces the Sherwood number by roughly a factor of two. In addition, the presence of multiple cells generally reduces horizontal density differences, as also apparent in comparing isopleths, leading to slower fluid speeds and weaker transport.

7. SUMMARY

In this study we have undertaken a combined theoretical and experimental program intended to help understand ion transport limitations and the effects of these limitations on electrodeposition for LIGA microdevice fabrication. Two numerical models have been developed: one describes either quasi-steady or transient one-dimensional diffusive transport of multiple ion species; the second describes two-dimensional diffusive and advective transport of a single species.

The first numerical model is implemented within a numerical framework that is readily adapted to a range of bath compositions, dissociation reactions, and electrode kinetics. To date we have focused on an eight-species model describing the simultaneous deposition of nickel and iron from a plating bath containing sulfuric acid and sulfates of both nickel and iron. The eight species presently included in the model are Fe^{2+} , FeOH^+ , Ni^{2+} , NiOH^+ , HSO_4^- , SO_4^{2-} , OH^- , and H^+ . In this model, transport of these ion species to the mold bottom is governed by diffusion, electromigration, and the homogeneous reactions between species as they move toward the deposition surface.

Experiments were conducted using a commercial 1.36 M (80 g/l) nickel sulfamate plating solution at a nominal temperature of 38 C. Current densities varying from about 100 to 1000 A/m² were applied to cathode molds having aspect ratios ranging from 1.6 to 25 over periods of approximately 24 hours. We found that surface morphology degraded significantly at the higher currents, and that larger aspect ratios produced poorer morphologies for a given current density. At an aspect ratio of 25, smooth uniform deposits were produced at currents up to about 300 A/m², but severe surface defects were observed at current densities of 400 A/m² and above. Current efficiencies were generally high for all of the test conditions, and efficiencies fell below 90% only at the highest current densities and feature aspect ratios.

The results of these experiments indicate that current densities well in excess of the diffusion limited currents may still yield acceptable morphologies in the deposited metal. This surprising result led to developing a second numerical model describing two dimensional convective motions within a single trench-like LIGA feature. The governing Navier Stokes equations include buoyancy forces resulting from ion depletion, as well as pressure, viscous and inertial forces. Although multiple species can be easily added, the current model includes only one transport equation describing diffusion and advection of a single metal species. The model was used to perform a series of numerical simulations over a range of external fluid speeds and fluid density variations typical of LIGA applications.

The results of these two-dimensional calculations first revealed that the experimentally observed hundred-fold increase in limiting currents cannot be attributed to fluid motion within the feature driven by external flow over the mold. Such flows produce a vertical stack of convective cells each having nearly unit aspect ratio. However, the maximum fluid speed in each successive cell falls by nearly three orders of magnitude, so fluid motion more than a few feature widths from the mold top is negligible for any practical fluid velocity outside the mold. Conversely, buoyancy-driven flows were found to have elongated convective cells with vertical speeds nearly independent of elevation within the feature. Such flows can easily account for the hundred-fold increase in limiting current observed in our experiments. Even at the smaller scale of LIGA features, transport rates and maximum current densities should exceed diffusion limits by more than an order of magnitude. Moreover, for sufficiently strong convection, plating rates should be independent of feature width and depth, a condition of great practical benefit to electroforming in the LIGA process.

ACKNOWLEDGMENT

This work was funded in part by a Sandia Phenomenological Modeling and Engineering Simulations LDRD, in part by a Materials Science and Technology LDRD, and in part by the Sandia Materials Science Research Foundation. Sandia is a multiprogram laboratory operated by Sandia Corporation, a Lockheed Martin Company, for the United States Department of Energy under contract DE-AC04-94AL85000.

REFERENCES

1. W. Ehrfeld and L. Lehr, "Deep X-Ray Lithographie for the Production of Three-Dimensional Microstructures from Metals, Polymers and Ceramics," *Radiat. Phys. Chem.*, **45** (3), pp. 349-365, 1995.
2. A. Maner, S. Harsch and W. Ehrfeld, "Mass Production of Microdevices with Extreme Aspect Ratios by Electroforming," *Plating and Surface Finishing*, pp. 60-65, March 1988.
3. A. Rogner, J. Eichert, D. Munchmeyer, R. P. Peters, and J. Mohr, "The LIGA Technique—What Are the New Opportunities" *J. Micromech. Microeng.*, **2**, pp. 133-140, 1992.
4. W. Ehrfeld and D. Munchmeyer, "Three-Dimensional Fabrication Using Synchrotron Radiation," *Nucl. Instrum. Methods Phys. Res.*, **A303**, pp. 523-531, 1991.
5. H. Guckel, "Deep X-Ray Lithographie for Micromechanics via Synchrotron Radiation," *Nucl. Instrum. Methods Phys. Res.*, **79** (1-4), pp. 247-248, 1993.
6. C. K. Malek, K. Jackson, R. A. Brennen, M. H. Hecht, W. D. Bonivert and J. M. Hruby, "Deep Etch X-Ray Lithography at the Advanced Light Source: First Results," EIPB '94, Proceeding of the 38th Int. Symp. on Electron, Ion and Proton Beams, New Orleans, LA, May 31-June 3, 1994.
7. Y. Fukunaka, H. Doi, and Y. Kondo, "Structural Variation of Electrodeposited Copper Film with the Addition of an Excess Amount of H₂SO₄," *J. Electrochem. Soc.*, **137** (1), pp. 88-93, 1990.
8. D. P. Barkey, R. H. Muller, and C. W. Tobias, "Roughness Development in Metal Electrodeposition," *J. Electrochem. Soc.*, **136** (8), pp. 2199-2214, 1989.
9. R. F. Probstein, *Physicochemical Hydrodynamics: An Introduction*, Second Edition, John Wiley & Sons, Inc., New York, 1994.
10. W. C. Grande and J. B. Talbot, "Electrodeposition of Thin Films of Nickel-Iron: II. Modeling," *J. Electrochem. Soc.*, **140** (3), pp. 675-681, 1993.
11. S. Hessami and C. W. Tobias, "A Mathematical Model for Anomalous Codeposition of Nickel-Iron on a Rotating Disk Electrode," *J. Electrochem. Soc.*, **136** (12), pp. 3611-3616, 1989.
12. S. K. Griffiths, R. H. Nilson, A. Ting, R. W. Bradshaw, W. D. Bonivert and J. M. Hruby, "Modeling Electrodeposition for LIGA Microdevice Fabrication," *Microsystems Technologies*, **4** (2), pp. 98-101, 1998.
13. N. Isaev and J. G. Osteryoung, "Thermoconvection-Enhanced Deposition of Copper," *J. Electrochem. Soc.*, **142** (12), pp. 4103-4107, 1995.
14. K. G. Jordan and C. W. Tobias, "Simulation of the Role of Convection in Electrodeposition into Microscopic Trenches," *J. Electrochem. Soc.*, **138** (7), pp. 1933-1939, 1991.
15. K. Bade, K. Leyendecker, A. Thommes, W. Bacher, "Electroplating at High Aspect Ratio Micropatterned Electrodes - Influence of Mass Transfer" Proc. Fourth Intl. Symposium on Magnetic Materials, Processes, and Devices, Electrochemical Society Fall Meeting, 1995.
16. J. J. L. Higdon, "Stokes Flow in Arbitrary Two-Dimensional Domains: Shear Flow over Ridges and Cavities," *J. Fluid Mech.*, **159**, pp. 195-226, 1985.
17. B. J. Gebhart, Y. Jaluria, R. L. Mahajan, and B. Sammakia, *Buoyancy-Induced Flows and Transport: Textbook Edition*, Hemisphere Publishing Corporation, New York, 1988.
18. A. K. Prasad and J. R. Koseff, "Combined Forced and Natural Convection Heat Transfer in a Deep Lid-Driven Cavity Flow," *Int. J. Heat and Fluid Flow*, **17**, pp. 460-467, 1996.